The electronic excited states of dichloromethane in the 5.8-10.8 eV energy range investigated by experimental and theoretical methods

E. Lange, N.C. Jones, S.V. Hoffmann, A.I. Lozano, S. Kumar, M.G.P. Homem, M.A. Śmialek, D. Duflot, M.J. Brunger, P. Limão-Vieira

The electronic excited states of dichloromethane in the 5.8-10.8 eV energy range investigated by experimental and theoretical methods

E. Lange,[1] N. C. Jones,[2] S. V. Hoffmann,[2] A. I. Lozano,[1] S. Kumar,[1]
M. G. P. Homem, [3] M. A. Śmiałek,[4] D. Duflot,[5,6*] M. J. Brunger,[7,8] P. Limão-Vieira,[1*]

[1] Atomic and Molecular Collisions Laboratory, CEFITEC, Department of Physics, Universidade NOVA de Lisboa, 2829-516 Caparica, Portugal

[2] ISA, Department of Physics and Astronomy, Aarhus University, Ny Munkegade, DK-8000, Århus C, Denmark

[3] Departamento de Química, Universidade Federal de São Carlos, 13565-905 São Carlos, São Paulo, Brazil

[4] Department of Control and Power Engineering, Faculty of Ocean Engineering and Ship Technology, Gdańsk University of Technology, Gabriela Narutowicza 11/12, 80-233 Gdańsk, Poland

[5] UMR 8523 - Physique des Lasers Atomes et Molécules, Univ. Lille, F-59000 Lille, France

[6] CNRS, UMR 8523, F-59000 Lille, France

[7] College of Science and Engineering, Flinders University, GPO Box 2100, Adelaide, SA 5001, Australia

[8] Dept. of Actuarial Science and Applied Statistics, Faculty of Business and Information Science UCSI, Kuala Lumpur 56000, Malaysia

ABSTRACT

We present a comprehensive experimental high-resolution vacuum ultraviolet (VUV) photoabsorption spectrum of dichloromethane, CH_2Cl_2, with absolute cross sections determined for the full 5.8–10.8 eV energy-range. The calculations on the vertical excitation energies and oscillator strengths were performed using the equation-of-motion coupled cluster method, restricted to the single and double excitations level (EOM-CCSD), and were used to help analyse the valence and Rydberg structures in the photoabsorption spectrum. The present spectrum additionally reveals several new features not previously reported in the literature, with particular reference to the valence $\sigma^*_{CCl}(10a_1) \leftarrow n_{Cl}(7b_2)$ $(1\ ^1B_2 \leftarrow \tilde{X}\ ^1A_1)$ and $(\sigma^*_{CCl}(10a_1) \leftarrow n_{Cl}(9a_1) + \sigma^*_{CH}(11a_1) \leftarrow n_{Cl}(7b_2))$ $(1\ ^1A_1 \leftarrow \tilde{X}\ ^1A_1)$ transitions at 7.519 and 7.793 eV. A vibrational progression of the CCl_2 symmetric stretching, ν_3', and CCl_2

scissoring, $\nu_4'(a_1)$, modes have also been assigned for the first time in the 7.4–8.6 eV energy range. The measured absolute photoabsorption cross sections have been used to calculate the photolysis lifetime of dichloromethane in the Earth's atmosphere (0–50 km). Potential energy curves as a function of the C–Cl coordinate, for the four lowest-lying excited A′ and A″ electronic states, have additionally been calculated at the EOM-CCSD level of theory.

Keywords: dichloromethane; Rydberg states; cross-sections; theoretical calculations; potential energy curves

[*] Corresponding authors:
P. Limão-Vieira. Tel: (+351) 21 294 78 59; Email: plimaovieira@fct.unl.pt (Paulo Limão-Vieira); Denis Duflot. Tel: (351) 21 294 78 59; Email: denis.duflot@univ-lille1.fr

1. INTRODUCTION

Dichloromethane, CH_2Cl_2, is a volatile organic compound (VOC) that was not included under the 1987 Montreal protocol (and its amendments), on chlorine and bromine containing substances that deplete the ozone layer and therefore needs to be phased out. Yet CH_2Cl_2, considered now as an ozone depleting chemical compound, has been widely used as an industrial solvent and as a feedstock for HFC-32 (difluoromethane) production [1,2], with current estimated global emissions of ~1 Tg y^{-1} [1,2]. Other sources of dichloromethane have been identified from fossil-fuel combustion and incineration [3], with the anthropogenic contributions amounting to ≈ 70% of the total emissions [1]. Dichloromethane can also be released into the atmosphere from oceans, biogenic emissions and biomass burning [3]. The atmospheric primary sink mechanism occurs at the troposphere, through reactions with $^{\bullet}OH$ radicals that limit the CH_2Cl_2 lifetime to half a year [1], and *ca*. 2% reaching the stratosphere according to Graedel and Keene [4]. As a consequence of the environmental impact of VOCs, the photochemistry of such halogenated chemical compounds has attracted increasing attention within the international scientific community, in particular for the role of chlorine radicals released at such altitudes upon solar photolysis [5,6].

Recent surface and aircraft measurements, together with atmospheric model simulations for future CH_2Cl_2 growth scenarios, indicate that although it currently contributes modest anthropogenic emissions, the impact of dichloromethane on ozone has increased strikingly in recent years [2]. Thus, as a result of such a tendency, its impact may considerably affect the stratospheric ozone local chemistry, with Hossaini et al. [2] predicting more than a decade delay in the recovery of stratospheric ozone over Antarctica.

CH_2Cl_2 has been investigated by various experimental methods that seek to elucidate its physico-chemical properties. These include bond lengths and geometry [7], ultraviolet photoabsorption [8–14] and photodissociation [15,16], photon and multiphoton ionisation [17–19], photoelectron spectroscopy [20,21], photo-oxidation [22,23] and electron impact spectroscopies [24–34], with the most recent electron scattering measurement reported by Hlousek et al. [35] and the Madrid group [36] (and references therein), with a particular focus on elastic differential cross sections and its grand total cross section, respectively. We also note that dichloromethane has been explored by several theoretical methods with studies investigating its molecular orbitals and geometry [10,37,38], calculations on the vertical excitation energies of its neutral molecule [10] and photodissociation [39].

The present work is part of a larger research programme aimed at understanding the spectroscopy of volatile organic compounds (e.g. refs. [40–43]), and the role of these trace gases in atmospheric chemistry and physics, that we initiated more than a decade ago [44]. In this contribution we present a novel and comprehensive experimental investigation of CH_2Cl_2 electronic state spectroscopy, in a wide energy range from 5.8 eV up to 10.8 eV, combined with state-of-the art calculations at different levels of theory of the lowest-lying neutral and ionic states. This data represents the most accurate assessment of the electronic structure of dichloromethane to date, where our absolute photoabsorption cross-section values can be relied upon over the entire photon energy range investigated.

In the next section we present a brief summary of the structure and properties of CH_2Cl_2, whilst Section 3 is devoted to the computational details of our calculations that we used to help in our interpretation of the experimental data. In Section 4, a description of the present experimental methodology is given, while Section 5 provides a comprehensive description of the electronic-state spectroscopy of dichloromethane in the 5.8–10.8 eV photon energy region and compares the present data with any other available in the literature. Additionally, in Section 5, the absolute photoabsorption cross section data has been used to calculate the photolysis rates of CH_2Cl_2 in the troposphere and stratosphere. Finally, Section 6 includes a brief summary of our major findings and details some conclusions drawn from the present joint experimental and theoretical investigation.

2. STRUCTURE AND PROPERTIES OF DICHLOROMETHANE

In this section we are particularly interested in giving a summary of the CH_2Cl_2 electronic structure, this is relevant to help us interpret and assess the role of its main molecular states involved in the excitation features revealed in our photoabsorption spectrum. Dichloromethane is a C_{2v} symmetry molecule in the electronic ground state, and its structure is represented in Figure 1 with the corresponding bond lengths (Å) and angles (°) listed in Table 1. The calculated electron configuration of the $\tilde{X}\ ^1A_1$ ground state is: (a) core and inner valence orbitals $(1a_1)^2$ $(1b_2)^2$ $(2a_1)^2$ $(2b_2)^2$ $(3a_1)^2$ $(3b_2)^2$ $(4a_1)^2$ $(4b_2)^2$ $(5a_1)^2$ $(1a_2)^2$ $(1b_1{}^2)$; (b) valence orbitals $(6a_1)^2$ $(5b_2)^2$ $(7a_1)^2$ $(2b_1)^2$ $(8a_1)^2$ $(6b_2)^2$ $(2a_2)^2$ $(9a_1)^2$ $(7b_2)^2$ $(3b_1)^2$ (Supplementary Information (SI) Table S1). A close inspection of the ground-state MOs (see SI Figure S1) shows that the highest occupied molecular orbital (HOMO) is denoted as $3b_1$, the second highest (HOMO-1) is denoted by $7b_2$, the third highest (HOMO-2) is denoted as $9a_1$, and the fourth highest (HOMO-3) is denoted by $2a_2$. All have a Cl lone pair character. Note that Mandal et al. [10] have considered only the ten highest molecular orbitals (MOs) and that their HOMO-2 and HOMO-3 are in a reverse order relative to the present calculation (albeit lying close in energy), whereas our 24 outermost electron occupation numbers are in good agreement with the calculated MOs of Alcantara et al. [37]. Electronic excitations discussed within the context of this work are due to promotion of an electron from the (HOMO), (HOMO-1) and (HOMO-2) orbitals to the valence, Rydberg and mixed character orbitals (see Table 2). Additional calculated transition energies, oscillator strengths, and the main character of the wave functions are shown in Table 3 for the singlet and triplet states (CASPT2 and MRCI results).

Relevant to the present study, the main fundamental vibrational energy (and wavenumber) of CH_2Cl_2 in the ground state is 0.089 eV (717 cm^{-1}) for the CCl_2 symmetric stretching mode, $v_3'(a_1)$. Note that throughout this paper, for the assignments of the vibronic structure we will adopt the notation X_m^n, with m and n the initial and final vibrational states and X denotes the particular geometric change the molecule undergoes in the photoabsorption process. Further note that other modes active in the photoabsorption spectrum have been assigned to CCl_2 scissoring, $v_4'(a_1)$, CCl_2 rocking, $v_7'(b_1)$, and CH_2 scissoring, $v_2'(a_1)$, modes, where we have followed the same spectroscopic notation as in v_3'. The experimental work on the photodissociation dynamics of vibrationally excited CH_2Cl_2 molecules [45], reports a strong mixing along the C–H coordinate stretches and bends via Fermi resonances. Thus the normal mode description may lead to Fermi resonances, making assignments in the absorption spectrum particularly challenging.

The four lowest experimental adiabatic ionisation energies, needed to calculate the quantum defects associated with transitions to Rydberg orbitals, are here taken from Pradeep and Shirley [20] to be 11.320 eV $(3b_1)^{-1}$, 11.357 eV $(7b_2)^{-1}$, 12.152 eV $(2a_2)^{-1}$ and 12.271 eV $(9a_1)^{-1}$ (Table 4). However, we note that Tuckett et al. [21] threshold photoelectron spectrum suggest that the vertical ionisation energy (VIE) of $\tilde{X}^+$ lies above the VIE of $\tilde{A}^+$, whereas the corresponding adiabatic ionisation energies (AIE) are reversed. Additionally, Franck–Condon modelling of improved-resolution photoelectron bands yielded AIEs of the $\tilde{X}^+\ ^2B_2$ and $\tilde{A}^+\ ^2B_1$ bands to be (11.0 ± 0.2) and (11.317 ± 0.006) eV [21]. These values are significantly different from Pardeep and Shirley [20] (see Table 4). Notwithstanding, the B_2/B_1 labelling order may differ which is very common depending on the different *ab initio* codes used. A close inspection of the HOMO and the HOMO-1 in Figure S1 (SI) show that these MOs are very close and so an inversion is certainly possible. Yet, the equilibrium geometry of the ions correspond to the adiabatic values so the lowest adiabatic state should be considered as the ionic ground state of dichloromethane.

3. THEORETICAL METHODS

In order to help interpret and lend support to our classifications of the majority of dichloromethane's absorption features, *ab initio* calculations were performed with the MOLPRO package [46]. This enabled us to obtain the geometry (Table 1 and Fig. 1) and excitation energies (Tables 2 and 3), together with the vertical ionisation energies (Table 4). The ground state geometry was optimized at the frozen core CCSD(T) [47] level using Dunning's aug-cc-pV5Z atomic basis sets [48]. However, in order to be able to visualize the orbitals using the Molden program [49], the *h* and *i* orbitals were removed from the Dunning basis set (aug-cc-pV5Z basis set). The electronic spectra were subsequently computed at the EOM-CCSD level [50] at the obtained CCSD(T) geometry. For a better description of Rydberg excited states, a set of diffuse functions (6s, 6p, 4d), taken from Kaufmann et al. [51], was added to the original basis set of the Cl atom (denoted by the aug-cc-pV5Z(g)+R basis set). The oscillator strengths of the electric dipole transitions were calculated using the length gauge. In order to test the accuracy of the EOM-CCSD calculations, we have also performed computations with multiconfigurational methods (CASPT2 and MRCI with the aug-cc-pV5Z(g)+R basis set) on the lowest lying valence and triplet states using MOLPRO.

Finally, the lowest vertical ionisation energies of CH_2Cl_2 were also obtained at the restricted and unrestricted CCSD(T) and UCCSD(T) aug-cc-pV5Z levels [52], by using Koopman's theorem, and with the Partial Third Order (P3), at the CCSD(T)/aug-cc-pV5Z geometry, and the Outer Valence Green Functions (OVGF) propagator methods (Table 4).

4. EXPERIMENTAL METHOD

The high-resolution vacuum ultraviolet (VUV) photoabsorption spectrum of dichloromethane (Figs. 2–5 and Tables 5–8 for assignments) was recorded at the UV1 beam line of the ASTRID synchrotron facility at Aarhus University, Denmark. The experimental configuration has been described before [53] so that only a précis need be given here. Briefly, monochromatised synchrotron radiation with a resolution of ~0.08 nm, corresponding to 3 meV at the midpoint of the energy range studied, passes through a static gas sample that is filled with dichloromethane vapour. Light transmitted through the absorption cell passes through a transmission window (MgF_2), that sets the lower limit of detection (115 nm), and is detected by a photomultiplier tube (PMT). The dichloromethane sample absolute pressure in the absorption cell is monitored by a 1 Torr capacitance manometer (Setra model 774). In order to guarantee the absence of any saturation effects in the data recorded, the absorption cross-sections were carefully measured over the pressure range 0.04–1.30 mbar, with typical attenuations of less than 50%. Absolute photoabsorption cross-sections (σ in units of Mb ≡ 10^{-18} cm^2) were obtained using the Beer-Lambert attenuation law: $I_t = I_0 e^{-N\sigma l}$, where I_t is the light intensity transmitted through the gas sample, I_o is that through the evacuated cell, N the molecular number density of dichloromethane, and l the absorption path length (15.5 cm). Background scans were recorded with the cell evacuated. In order to accurately determine the cross-sections, the VUV spectrum was recorded in small (5 or 10 nm) sections, with at least 10 points overlap in each of the adjoining sections. This procedure allows us to determine the accuracy of the photoabsorption cross-section to within ± 5%.

The liquid sample used in the VUV photoabsorption measurements was purchased from Sigma Aldrich (cat. No. 270997), with a stated purity of ≥ 99.8%. This sample, before any photoabsorption experiments took place, was degassed after repeated freeze-pump-thaw cycles.

5. RESULTS AND DISCUSSION

The absolute high-resolution VUV photoabsorption cross-section of dichloromethane is shown in Figure 2, in the 5.8–10.8 eV photon energy range, with detailed sections of the measured cross-section depicted in Figures 3–5. The electronic excitation above 7.6 eV is extremely rich in fine structure, with the CCl_2 symmetric stretching mode, v_3', dominant for the entire energy range, and above 9.6 eV the observed structure is due to the overlap of different Rydberg electronic states contributing to the spectrum. The absorption bands are classified as excitations from the ground to valence, Rydberg (Section 5.5) and mixed character states of the type $(10a_1 \leftarrow 3b_1)$, $(10a_1 \leftarrow 7b_2)$, $(nsa_1, npa_1, npb_1, ndb_1 \leftarrow 3b_1)$, $(nsa_1, npa_1, npb_2, nda_1 \leftarrow 7b_2)$, $(npa_1, npa_1, nda_1 \leftarrow 9a_1)$, $(10a_1 \leftarrow 9a_1 + 11a_1 \leftarrow 7b_2)$ and $(10a_1 \leftarrow 2a_2 + 11a_1 \leftarrow 3b_1)$. Tables 5–7 show the energy values for the vibrational assignments in the different absorption bands of dichloromethane, and these are compared whenever possible with previous data in the literature. In particular we note the work of Mandal et al. [10], across the 6.0–11.5 eV energy range, although that study reports no absolute values. Based on the present experimental data and calculations, we now describe in detail each photon energy range.

5.1. The 5.8–7.4 eV photon energy range

This energy range (included within Figure 2) is characterised by two broad weak features, a band and a shoulder structure, peaking at 7.069 eV and 7.519 eV. Those features are assigned to valence $\sigma^*_{CCl}(10a_1) \leftarrow n_{Cl}(3b_1)\ (1\ ^1B_1 \leftarrow \tilde{X}\ ^1A_1)$ and $\sigma^*_{CCl}(10a_1) \leftarrow n_{Cl}(7b_2)\ (1\ ^1B_2 \leftarrow \tilde{X}\ ^1A_1)$ transitions, with local cross-section values of 1.9 and 2.4 Mb, respectively (see Table 2). The lowest intensity absorption band has previously been reported by Lee and Suto [15] and Mandal et al. [10] at ~ 7.085 eV and ~7.0 eV, respectively, yet with assignments differing from the present work, whereas Russell et al. [11] report this feature at 7.042 eV but with an oscillator strength of 0.05 which is clearly too high for the nature of the $\sigma^*_{CCl} \leftarrow n_{Cl}$ transition. Moreover, this band has been also the subject of 193.3 nm (6.415 eV) photodissociation dynamics studies by Brownsword et al. [54] and Taketani et al. [16]. In the former case the authors report a low efficiency in C–H bond cleavage with a quantum yield of $\varphi_H(CH_2Cl_2) = (0.2 \pm 0.1)\times10^{-2}$, and in the latter work a quantum yield of Cl-atom formation of unity was found. Other absorption studies include the UV work of Gordus and Bernstein [8] and Hubrich and Stuhl [9], but with information only on the cross-section value at 5.815 eV and in the 4.862–7.746 eV energy range being given, respectively (see Section 5.6).

In order to test the level of accuracy for the results of our calculations in Table 2, we have employed other levels of theory using multiconfigurational methods, CASPT2 [55,56] and internally contracted MRCI [57] with the aug-cc-pV5Z(g)+R basis set, in order to obtain the low-lying valence singlet and triplet states of dichloromethane. This is in spite of the VUV photoabsorption data in Figure 2 being related to only optically allowed transitions. The results of those latter calculations are presented in Table 3, and compared with the other available data in the literature. For the singlet excitations, the present results are in much better agreement with the experimental data. Furthermore they are higher in energy than the results from the calculations performed by Mandal et al. [10], by 0.5 eV at the TD-PBE0 level, and with those of Xiao et al. [39], at the CASPT2 level, possibly due to their [37] smaller basis set and/or active space used. The calculated lowest singlet transitions at the MS-CASPT2(20,14)/aug-cc-pV5Z(g) and the MS-CAS(20,14)+icMRCI+Q/aug-cc-pV5Z(g) levels, give best agreement with the experimental values. This table also shows that the EOM-CCSD/aug-cc-pV5Z(g)+R method is accurate while allowing to obtain a much larger number of excited states compared to multiconfigurational techniques.

The VUV absorption data are typically related to optically allowed transitions, although the low-intensity feature at 7.069 eV (with a calculated f = 0.00024, see Table 2) may be related to optically forbidden transitions. We note that in a previous comprehensive investigation of the *A*-band low-lying electronic states in the methyl halides CH_3X (X = F, Cl, Br and I), by electron impact excitation [58], the (n → σ*) transitions involved the excitation of both singlet and triplet states. The lowest valence triplet transition energy, calculated at the MS-CASPT2(20,14)/aug-cc-pV5Z(g) level and MS-CAS(20,14)+icMRCI+Q/aug-cc-pV5Z(g) level, assign that feature at 6.644 and 6.750 eV, respectively, while the MS-CAS(20,14)/aug-cc-pV5Z(g) calculation predicts a value at a higher energy, 7.201 eV. Those discrepancies between the results of our most accurate calculations, as far as dichloromethane is concerned, suggest that further electron scattering experiments are certainly needed to clarify the role of such underlying states. This follows as the corresponding spectral features can be probed under conditions more favourable for optically forbidden transitions, namely at lower energy electron impact and for higher electron scattering angles [59].

5.2. The 7.4–8.6 eV photon energy range

The structureless features in this band have been reported before, in the experimental works of Russell et al. [11] and Mandal et al. [10], as arising from (4s ← n) Rydberg transitions converging to the ionisation energies. The current photoabsorption spectrum is presented in Figure 3, with our proposed assignments summarised in Tables 2 and 8. Note that the present calculations indicate that this energy region is characterised by a contribution of valence and Rydberg transitions (see Section 5.5). The lowest-lying excited state of dichloromethane in this energy region is tentatively placed at 7.793 eV, with a local cross-section value of 5.0 Mb. We have assigned this to the $\left(\sigma^*_{CCl}(10a_1) \leftarrow n_{Cl}(9a_1) + \sigma^*_{CH}(11a_1) \leftarrow n_{Cl}(7b_2)\right)$ $\left(1\ {}^1A_1 \leftarrow \tilde{X}\ {}^1A_1\right)$ transition, with an oscillator strength of ~0.0047 (Table 2), and it shows for the first time some weak fine structure reminiscent of the pre-dissociative character of the absorption band. The 0^0_0 origin band is tentatively assigned at 7.72(0) eV, with a 3^n_0 (n = 0–2) progression of the CCl_2 symmetric stretching mode, ν'_3, and an average spacing of 0.078 eV (629 cm^{-1}). However, a contribution from the CCl_2 scissoring mode, $\nu'_4(a_1)$, is also discernible (see Table 5). Other progressions at higher energy have also been assigned and are discussed in detail in Section 5.5 for the Rydberg transitions.

5.3. The 8.5–9.7 eV photon energy range

This energy range accommodates the third absorption band of dichloromethane (Figure 4) and is comprised of both valence and Rydberg transitions (Section 5.5). Russell et al. [11] reported an absorption band at 9.076 eV, assigned to (4p,3d ← n) transitions, while Mandal et al. [10] reported members of Rydberg series converging to the three lowest ionic states.

According to the results of our calculations presented in Table 2, the valence transitions in this energy range have been respectively assigned to $\left(\sigma_{CCl}^{*}(10a_1) \leftarrow n_{Cl}(2a_2) + \sigma_{CH}^{*}(11a_1) \leftarrow n_{Cl}(3b_1)\right)$ $\left(4\ {}^{1}B_1 \leftarrow \tilde{X}\ {}^{1}A_1\right)$ and $\sigma_{CCl}^{*}(8b_2) \leftarrow n_{Cl}(9a_1)$ $\left(4\ {}^{1}B_2 \leftarrow \tilde{X}\ {}^{1}A_1\right)$, peaking at 9.123 eV and 9.585 eV, with maximum cross-section values of 49.5 and 49.7 Mb. The 0_0^0 origin bands are at 8.67(6) eV and 9.508 eV, with the spectral assignments being contained in Table 6 and with the observed progressions assigned to the CCl_2 symmetric stretching, $\nu_3'(a_1)$, and CCl_2 scissoring, $\nu_4'(a_1)$, modes. This indicates that the structure description is complex, due to the strong Fermi resonances between these two vibrations. The average excited state frequencies of the ν_3'- and ν_4'-modes in the valence transition are 0.076 eV and 0.027 eV, with ground-states values of 0.089 eV (717 cm^{-1}) and 0.035 eV (282 cm^{-1}). Lee and Suto [15] also reported progressions for the CCl_2 symmetric stretching, ν_3', and for the CH_2 twisting, ν_5', modes. Regarding the latter, we have not attempted any spectral assignment given its a_2 symmetry.

5.4. Ionisation energies of dichloromethane

Table 4 lists the calculated vertical ionisation energies (*IE*s) for dichloromethane, at different levels of theory, and are compared with the experimental values available in the literature. A close inspection of the tabulated values reveals that all the theoretical methods agree reasonably well with each other while those provided by the Koopmans' theorem [60] are larger in value. Such a difference is not surprising in view of the improper electron correlation (and relaxation) treatment in Koopmans' theorem. In order to assign the lowest lying Rydberg members converging to the ionic electronic ground ($3b_1^{-1}$), first ($7b_2^{-1}$), second ($2a_2^{-1}$) and third ($9a_1^{-1}$) excited states, we have used the experimental adiabatic IE values of 11.320 eV, 11.357 eV, 12.152eV and 12.271 eV (Table 4).

5.5. Rydberg transitions and the 9.6–10.8 eV photon energy range

The VUV photoabsorption spectrum above 7.6 eV displays a prominent Rydberg character (Figures 3–5), where a summary of the experimental energies, proposed assignments and quantum defects can be found in Table 8. The peak positions have been tested using the Rydberg formula: $E_n = IE - R/(n-\delta)^2$, where *IE* is the ionisation energy, *n* is the principal quantum number of the Rydberg orbital of energy E_n, *R* is the Rydberg constant (13.61 eV), and δ is the quantum defect resulting from the penetration of the Rydberg orbital into the core. The Rydberg structures of dichloromethane have been analysed previously [10,11,14,15,61], yet there remain discrepancies in some of the former assignments which deserve a comprehensive investigation such as we report here. A summary of the calculated Rydberg transitions is tabulated in the Supplementary Information (Table S2) and compared with Mandal et al. [10]. We observe large differences in their calculated values (from 0.5 eV up to 1 eV), which are very likely due to the lack of very diffuse functions in the basis set used for the description of high-n Rydberg states.

The lowest-lying Rydberg transition is assigned to $(nsa_1 \leftarrow 3b_1)\ \left({}^2B_1 \leftarrow \tilde{X}\ {}^1A_1\right)$, with the first member $n = 4$ at 7.72(0) eV and having a quantum defect $\delta = 2.06$ (Table 8). That energy is in good agreement with the 7.7 eV value from the experimental data of Mandal and co-workers [10]. Transitions to the n = 5–7 members of the nsa_1 series are also in reasonably good accord with previous experimental data [10]. The first members of the two n*p* ($npb_1 \leftarrow 3b_1$) / ($npa_1 \leftarrow 3b_1$) and one n*d* ($ndb_1 \leftarrow 3b_1$) series are associated with peaks at 8.837 eV and 9.294 eV (δ = 1.66 and 1.41) and 9.61(1) eV (δ =0.18), and are accompanied by several quanta of the ν_3'- and ν_4'-modes (Tables 5 and 7). For the higher order members of the Rydberg series (n > 6), we have not made any attempt to identify their features due to their low intensity in the absorption spectrum.

The Rydberg series converging to the ionic first excited electronic state are listed in Table 8, and have been assigned to the $(nsa_1, npa_1/npb_2, nda_1 \leftarrow 7b_2)\ \left({}^2B_2 \leftarrow \tilde{X}\ {}^1A_1\right)$ transitions. The first members of the *ns*, *np* and *nd* series are associated with features at 7.96(3) eV (δ =1.99), 8.952/9.75(9) eV (δ =1.62/1.08) and 7.75(9) eV (δ =0.08). Note that the early measurements of Russell et al. [11] reported an absorption band at 8.217 eV and a shoulder at 7.978 eV assigned to two degenerate (4*s* ← *n*) transitions, although our calculations in Table 2 do not lend support to their classification for those latter two states. The present Rydberg (tentative) assignments have been made up to n = 6, where some of the features contribute to more than one series. Such a contribution may be discernible from a close inspection of the VUV spectrum, where such peaks tend to appear broader due to contributions from vibrational modes (Tables 6 and 7). The extensive vibrational excitation of mode ν_4' in the lowest-lying Rydberg state n = 4*s*, is in good accord with the fine structure found in the He(I) photoelectron spectrum of Pradeep et al. [20].

Regarding the Rydberg series $(nsa_1, npa_1, nda_1 \leftarrow 2a_2)\ \left({}^2A_2 \leftarrow \tilde{X}\ {}^1A_1\right)$ of dipole forbidden transitions, converging to the ionic second excited electronic state, the values in Table 8 are part of vibronic transitions and/or superposition with other Rydberg series.

As far as the members of the Rydberg series converging to the third ionic excited electronic state are concerned, n = 4 for ns, np and nd, we propose that they are located in our photoabsorption spectrum at 8.67(6)/8.756 eV, 9.899 eV and 10.670 eV (Table 8) with quantum defects 2.05/2.03, 1.60 and 0.08, respectively. Some of the observed fine structure in those lines has been assigned to vibrational excitation involving the CCl_2 symmetric stretching mode, $v_3'(a_1)$, the CCl_2 scissoring mode, $v_4'(a_1)$, and the CCl_2 rocking, $v_7'(b_1)$, mode (see Tables 6 and 7).

5.6. Absolute photoabsorption cross sections and atmospheric photolysis

Previous absolute VUV photoabsorption cross sections of dichloromethane are available in the wavelength range 111–200 nm (6.199–11.169 eV) [11], 110–210 nm (5.904–11.271 eV) [15], 160–255 nm (4.862–7.749 eV) [9] and 176–220 nm (5.636–7.044 eV) [12]. Those measurements were conducted at specific temperatures in the 210–295 K range.

From the data of Russell et al. [11] the vertical excitation of the lowest-lying excited state at 7.069 eV yields a photoabsorption cross-section of 0.003 Mb, compared to our cross-section value of 1.9 Mb. On the other hand Hubrich et al. [9] and Lee and Suto [15] reported at 175 nm (7.085 eV) cross-section values of 1.87 and ~1.75 Mb, in good agreement with our value of 1.90 Mb. Furthermore, at 295 K, Simon et al. [12] reported at 186 nm (6.666 eV) a cross-section value of 1.04 Mb, in good accord with the present value of 1.04 Mb. Finally, two other experimental values from optical absorption experiments reported cross-section values at 193.3 nm (6.414 eV) and 213.2 nm (5.815 eV) of 0.37 Mb [54] and 0.009 Mb [8], respectively, while we correspondingly found the values to be ~0.32 Mb and 0.004 Mb from the present experiments (see Figure 2).

High-resolution VUV absolute photoabsorption cross sections, in combination with solar actinic flux measurements from the literature [62], can be used to calculate the photolysis rates of dichloromethane in the Earth's atmosphere (0–50 km altitude) through a simple methodology as described in Ref. [63]. The quantum yield for dissociation, mainly in Cl-atom release, is assumed to be unity from the work of Taketani et al. [16]. Photolysis lifetimes of less than a week in sunlit days were calculated at altitudes above 40 km. This indicates that dichloromethane molecules are efficiently broken up by VUV absorption at these altitudes, contributing therefore to stratospheric halogen loading. At lower altitudes the photolysis lifetimes are, however, very high, meaning that these molecules cannot be broken up by UV radiation. Alapi and Dombi [22] reported a comprehensive study of gas-phase CH_2Cl_2 reactions with $Cl^{\bullet}$ and $^{\bullet}OH$ radicals, with rate constant values of $k_{Cl} = 3.67\times10^{-13}$ cm^3

molecule^{-1} s^{-1} and k_{OH} = 1.26×10^{-13} cm^3 molecule^{-1} s^{-1}, while Yu et al. [23] have shown the efficiency of CH_2Cl_2 photodegradation, by a combination of VUV light, ozone and hydroxyl radicals oxidation through the main intermediates detected. Thus, compared with these reactions, UV photolysis is not expected to play a significant role in the tropospheric removal of CH_2Cl_2 molecules.

5.7. Potential energy curves along the CH_2Cl_2 → CH_2Cl + Cl coordinate

We have performed calculations of the potential energy curves (PECs) along one of the C–Cl bonds, at the EOM-CCSD/aug-cc-pV5Z(g)+R level of theory in the C_s symmetry group, while keeping the other geometric parameters fixed at their values obtained from the CCSD(T)/aug-cc-pV5Z level computations. The four lowest-lying excited A′ and A″ states and their character are presented in Figure 6, with their energy values being given in Table 9. Mandal et al. [10] have calculated similar PECs using density functional theory, with the PBE0/6-311G+(2d, 2p) basis set. Differences between the present results and those of Mandel et al. are noted at some of the asymptotic limits, as well as in the representation of the curve crossings. Such differences may arise from the level of theory used in the present calculations. A close inspection of the PECs in Figure 6 show a large number of avoided crossings, implying multiple conical intersections in the full multi-dimensional space. The first two excited states, n_{Cl} ($3b_1$) → σ_{CCl}* ($10a_1$) and n_{Cl} ($7b_2$) → σ_{CCl}* ($10a_1$), are almost degenerate because the HOMO (n_{Cl}) and HOMO-1 (n_{Cl}) are also degenerate even at short distances. These states show a clear dissociative character, which can explain the absence of any clear fine structure in the 7.0–7.6 eV energy region of the VUV photoabsorption spectrum. Regarding the higher energy valence states, the bond breaking through C–Cl and/or C–H coordinates stands to be proven which implies that another complex underlying molecular mechanism, e.g. conical intersections, may be responsible for the dissociative dynamical character. The role of Rydberg states, related to Cl-atom release relevant to stratospheric ozone local chemistry, are not evident from the PECs. These may therefore require in the future a full optimization for each of these states, at a more computationally expensive level of theory, which is beyond the focus of this contribution.

6. CONCLUSIONS

We have presented a comprehensive investigation of the VUV electronic-state spectroscopy of dichloromethane in the 5.8–10.8 eV energy range, with the most reliable and complete set of absolute photoabsorption cross-sections for this region being given. The main absorption features are due to electronic excitations from the ground state to valence, Rydberg and mixed-character states. Novel assignments have been made, which have not been previously reported in the literature. Theoretical calculations on the vertical excitation energies and oscillator strengths were performed using the equation-of-motion coupled cluster method, but were restricted to the single and double excitation level in order to help in our assigning of the valence and Rydberg transitions.

The present photoabsorption spectrum revealed several new features not previously reported, with valence $\sigma^*_{CCl}(10a_1) \leftarrow n_{Cl}(7b_2)\,(1\ ^1B_2 \leftarrow \tilde{X}\ ^1A_1)$ and $(\sigma^*_{CCl}(10a_1) \leftarrow n_{Cl}(9a_1) + \sigma^*_{CH}(11a_1) \leftarrow n_{Cl}(7b_2))\,(1\ ^1A_1 \leftarrow \tilde{X}\ ^1A_1)$ transitions at 7.519 and 7.793 eV being a good example of this. The analysis of the observed vibronic structure in the photoabsorption spectra also allowed us to propose, for the first time, assignments for the CCl_2 symmetric stretching, v'_3, and CCl_2 scissoring, $v'_4(a_1)$, modes. The photolysis lifetimes of dichloromethane were also derived for the Earth's troposphere and stratosphere, as a part of this investigation, and showed that solar photolysis is expected to be a weak sink in the terrestrial atmosphere. Finally potential energy curves as a function of the C–Cl coordinate, for the four lowest-lying excited A′ and A″ states, were calculated at the EOM-CCSD level of theory with aug-cc-pV5Z(g)+R basis set.

AUTHOR INFORMATION

Corresponding Authors

*(P.L.-V.) E-mail: plimaovieira@fct.unl.pt

*(D. Duflot) Email: denis.duflot@univ-lille1.fr

ORCID

E. Lange: 0000-0002-9279-8210

N. C. Jones: 0000-0002-4081-6405

S. V. Hoffmann: 0000-0002-8018-5433

A. I. Lozano: 0000-0003-4613-0372

S. Kumar: 0000-0002-1996-9925

M. Homem: 0000-0002-6640-664X

M. A. Śmiałek: 0000-0003-2624-3716

M. J. Brunger: 0000-0002-7743-2990

D. Duflot: 0000-0002-8307-5344

P. Limão-Vieira: 0000-0003-2696-1152

Notes

The authors declare no competing financial interest.

ACKNOWLEDGMENTS

E.L. acknowledges the Brazilian Agency Conselho Nacional de Desenvolvimento Científico e Tecnológico (CNPq) and the Science Without Borders Programme for opportunities to study abroad. S.K. acknowledges the Portuguese National Funding Agency FCT through Researcher PD/BD/142831/2018, and, together with A.I.L. and P.L.V., the Research Grants CEFITEC (UIDB/00068/2020) and PTDC/FIS-AQM/31281/2017. This work was also supported by the Radiation Biology and Biophysics Doctoral Training Programme (RaBBiT, PD/00193/2012); UCIBIO (UIDB/04378/2020). The research leading to these results has received funding from the European Community's Seventh Framework Programme (FP7/2007-2013) under grant agreement nº 226716. DD acknowledges the support of the OVERSEE and CAPPA grants, managed by the Agence Nationale de la Recherche under the frame programs Investissements dAvenir ANR-10-LABX-005 and I-SITE ULNE/ANR-16-IDEX-0004 ULNE, respectively. D.D. also thanks the Région Hauts de France, the Ministre de lEnseignement Suprieur et de la Recherche (CPER Climibio) and the European Fund for Regional Economic Development for their support. This work used HPC resources from GENCITGCC (Grant No. 2019-A0010806820) and the Centre de Ressources Informatiques (CRI) of the Université de Lille. Partial financial support from the Australian Research Council through grant DP180101655 is also acknowledged.

REFERENCES

[1] Simmonds PG, Manning AJ, Cunnold DM, McCulloch A, O'Doherty S, Derwent RG, et al. Global trends, seasonal cycles, and European emissions of dichloromethane, trichloroethene, and tetrachloroethene from the AGAGE observations at Mace Head, Ireland and Cape Grim, Tasmania. J Geophys Res Atmos 2006;111:1–19. https://doi.org/10.1029/2006JD007082.

[2] Hossaini R, Chipperfield MP, Montzka SA, Leeson AA, Dhomse SS, Pyle JA. The increasing threat to stratospheric ozone from dichloromethane. Nat Commun 2017;8:1–9. https://doi.org/10.1038/ncomms15962.

[3] Keene WC, Khalil MAK, Erickson DJ, McCulloch A, Graedel TE, Lobert JM, et al. Composite global emissions of reactive chlorine from anthropogenic and natural sources: Reactive chlorine emissions inventory. J Geophys Res 1999;104:8429–40. https://doi.org/10.1029/1998JD100084.

[4] Graedel TE, Keene WC. The budget and cycle of Earth's natural chlorine. Pure Appl Chem 1996;68:1689–97. https://doi.org/10.1351/pac199668091689.

[5] Molina MJ, Rowland FS. Stratospheric sink for chlorofluoromethanes: chlorine atom-catalysed destruction of ozone. Nature 1974;249:810–2. https://doi.org/10.1038/249810a0.

[6] Rowland FS, Molina J. Chlorofluoromethanes in the Environment. Rev Geophys Sp Phys 1975;13:1–35. https://doi.org/10.1029/RG013i001p00001.

[7] Berry RJ, Harmony MD. The use of scaled moments of inertia in experimental structure determinations of polyatomic molecules. Struct Chem 1990;1:49–59. https://doi.org/10.1007/BF00675784.

[8] Gordus AA, Bernstein RB. Isotope effect in continuous ultraviolet absorption spectra: Methyl bromide-d3 and chloroform-d. J Chem Phys 1954;22:790–5. https://doi.org/10.1063/1.1740194.

[9] Hubrich C, Stuhl F. The ultraviolet absorption of some halogenated methanes and ethanes of atmospheric interest. J Photochem 1980;12:93–107. https://doi.org/10.1016/0047-2670(80)85031-3.

[10] Mandal A, Singh PJ, Shastri A, Jagatap BN. Vacuum ultraviolet photoabsorption spectroscopy of CH2Cl2 and CD2Cl2 in the energy region 50,000-95,000 cm-1. J Quant Spectrosc Radiat Transf 2014;149:291–302. https://doi.org/10.1016/j.jqsrt.2014.08.015.

[11] Russell BR, Edwards LO, Raymonda JW. Vacuum Ultraviolet Absorption Spectra of

the Chloromethanes. J Am Chem Soc 1973;95:2129–33. https://doi.org/10.1021/ja00788a008.

[12] Simon PC, Gillotay D, Vanlaethem-Meuree N, Wisemberg J. Ultraviolet absorption cross-sections of chloro and chlorofluoro-methanes at stratospheric temperatures. J At Chem 1988;7:107–35. https://doi.org/10.1007/BF00048042.

[13] Tsubomura H, Kimura K, Kaya K, Tanaka J, Nagakura S. Vacuum Ultraviolet Absorption Spectra of Saturated Organic Compounds with Non-bonding Electrons. B Chem Soc Jpn 1964;37:417–23.

[14] Zobel CR, Duncan ABF. Vacuum Ultraviolet Absorption Spectra of Some Halogen Derivatives of Methane. Correlation of the Spectra. J Am Chem Soc 1955;77:2611–5. https://doi.org/10.1021/ja01614a084.

[15] Lee LC, Suto M. Fluorescence yields from photodissociative excitation of chloromethanes by vacuum ultraviolet radiation. Chem Phys 1987;114:423–9. https://doi.org/10.1016/0301-0104(87)85056-5.

[16] Taketani F, Takahashi K, Matsumi Y. Quantum yields for Cl(2Pj) atom formation from the photolysis of chlorofluorocarbons and chlorinated hydrocarbons at 193.3 nm. J Phys Chem A 2005;109:2855–60. https://doi.org/10.1021/jp044218+.

[17] Lago AF, Kercher JP, Bödi A, Sztáray B, Miller B, Wurzelmann D, et al. Dissociative photoionization and thermochemistry of dihalomethane compounds studied by threshold photoelectron photoion coincidence spectroscopy. J Phys Chem A 2005;109:1802–9. https://doi.org/10.1021/jp045337s.

[18] Chiang SY, Bahou M, Sankaran K, Lee YP, Lu HF, Su M Der. Dissociative photoionization of CH2Cl2 and enthalpy of formation of CHCl+: Experiments and calculations. J Chem Phys 2003;118:62–9. https://doi.org/10.1063/1.1524178.

[19] Werner AS, Tsai BP, Baer T. Photoionization study of the ionization potentials and fragmentation paths of the chlorinated methanes and carbon tetrabromide. J Chem Phys 1974;60:3650–7. https://doi.org/10.1063/1.1681585.

[20] Pradeep T, Shirley DA. High resolution photoelectron spectroscopy of CH2Cl2 and CF2Cl2 using supersonic molecular beams. J Electron Spectrosc Relat Phenom 1993;66:125–38. https://doi.org/10.1016/0009-2614(93)85059-W.

[21] Tuckett R, Harvey J, Hemberger P, Bodi A. The vacuum-ultraviolet photoelectron spectra of CH2F2 and CH2Cl2 revisited. J Mol Spectrosc 2015;315:172–83. https://doi.org/10.1016/j.jms.2015.02.012.

[22] Alapi T, Dombi A. Direct VUV photolysis of chlorinated methanes and their mixtures

in an oxygen stream using an ozone producing low-pressure mercury vapour lamp. Chemosphere 2007;67:693–701. https://doi.org/10.1016/j.chemosphere.2006.10.066.

[23] Yu J, Cai W, Chen J, Feng L, Jiang Y, Cheng Z. Conversion characteristics and mechanism analysis of gaseous dichloromethane degraded by a VUV light in different reaction media. J Environ Sci 2012;24:1777–84. https://doi.org/10.1016/S1001-0742(11)61021-8.

[24] Scheunemann H-U, Illenberger E, Baumgartel H. Dissociative Electron Attachment to CCl4, CHCl3, CH2C12 and CH3Cl. Ber Bunsenges Phys Chem 1980;84:580–5.

[25] Pearl DM, Burrow PD. Dissociative attachment in selected monochloroalkanes. J Chem Phys 1994;101:2940–8. https://doi.org/10.1063/1.467606.

[26] Bart M, Harland PW, Hudson JE, Vallance C. Absolute total electron impact ionization cross-sections for perfuorinated hydrocarbons and small halocarbons. Phys Chem Chem Phys 2001;3:800–6.

[27] Natalense APP, Bettega MHF, Ferreira LG, Lima MAP. Halogenation effects in electron scattering from CHF3,CH2F2,CH3F, CHCl3,CH2Cl2, CH3Cl, CFCl3,CF2Cl2, and CF3Cl. Phys Rev A 1999;59:879–81.

[28] Naghma R, Gupta D, Goswami B, Antony B. Electron impact ionization cross sections for chlorinated and brominated methane and CnH2n+1Cl (where n = 2 , 3 , 4) molecules. Int J Mass Spectrom 2014;360:39–44. https://doi.org/10.1016/j.ijms.2013.12.019.

[29] Naghma R, Gupta D, Antony B. Total cross sections for electron scattering with halocarbon molecules. J Electron Spectrosc Relat Phenom 2014;193:48–53. https://doi.org/10.1016/j.elspec.2014.03.003.

[30] Krupa K, Lange E, Blanco F, Barbosa AS, Pastega DF, Sanchez SD, et al. Experimental and theoretical electron-scattering cross-section data for dichloromethane. Phys Rev A 2018;97:042702. https://doi.org/10.1103/PhysRevA.97.042702.

[31] Hudson JE, Vallance C, Bart M, Harland PW. Absolute electron-impact ionization cross sections for a range of C1 to C5 chlorocarbons. J Phys B At Mol Opt Phys 2001;34:3025–39.

[32] Gallup GA, Fabrikant II. Dissociative electron attachment to CH2Cl2, CHCH3Cl2, and C(CH3)2Cl2. J Chem Phys 2011;135:134316. https://doi.org/10.1063/1.3646500.

[33] Burns SJ, Matthews JM, Mcfadden DL. Rate Coefficients for Dissociative Electron Attachment by Halomethane Compounds between 300 and 800 K. J Phys Chem 1996;100:19436–40. https://doi.org/10.1021/jp962529h.

[34] Benitez A, Moore JH, Tossell JA. The correlation between electron transmission and inner shell electron excitation spectra. J Chem Phys 1998;88:6691–8. https://doi.org/10.1063/1.454413.

[35] Hlousek BA, Martin MF, Zawadzki M, Khakoo MA, Machado LE, Lucchese RR, et al. Low to intermediate energy elastic electron scattering from dichloromethane (CH2Cl2). J Phys B At Mol Opt Phys 2019;52:025204. https://doi.org/10.1088/1361-6455/aaf2f4.

[36] Lozano AI, Álvarez L, Blanco F, Brunger MJ, García G. Total cross section measurements for electron scattering from dichloromethane. J Chem Phys 2018;149:244304. https://doi.org/10.1063/1.5080636.

[37] Alcantara KF, Wolff W, Gomes AHA, Sigaud L, Soriano S, Oliveira V, et al. Fragmentation of the CH2Cl2 molecule by proton impact and VUV photons. J Phys B At Mol Opt Phys 2011;44:165205. https://doi.org/10.1088/0953-4075/44/16/165205.

[38] Xi HW, Huang MB. The 12B2, 12B1, 12A1, 12A2, and 32A′(22B2) states of the 1,1-dichloromethene ion studied using multiconfiguration second-order perturbation theory. Chem Phys Lett 2006;425:28–34. https://doi.org/10.1016/j.cplett.2006.05.012.

[39] Xiao HY, Liu YJ, Yu JG, Fang WH. Spin-orbit ab initio investigation of the photodissociation of CH2Cl2. Chem Phys Lett 2007;436:75–9. https://doi.org/10.1016/j.cplett.2007.01.053.

[40] Śmiałek MA, Hubin-Franskin MJ, Delwiche J, Duflot D, Mason NJ, Vrønning-Hoffmann S, et al. Limonene: Electronic state spectroscopy by high-resolution vacuum ultraviolet photoabsorption, electron scattering, He(i) photoelectron spectroscopy and ab initio calculations. Phys Chem Chem Phys 2012;14:2056–64. https://doi.org/10.1039/c2cp22847e.

[41] Martins G, Ferreira-Rodrigues AM, Rodrigues FN, de Souza GGB, Mason NJ, Eden S, et al. Valence shell electronic spectroscopy of isoprene studied by theoretical calculations and by electron scattering, photoelectron, and absolute photoabsorption measurements. Phys Chem Chem Phys 2009;11:11219–31. https://doi.org/10.1039/b916620c.

[42] Serralheiro C, Duflot D, da Silva FF, Hoffmann SV, Jones NC, Mason NJ, et al. Toluene Valence and Rydberg Excitations as Studied by ab initio Calculations and Vacuum Ultraviolet (VUV) Synchrotron Radiation. J Phys Chem A 2015;119:9059–69. https://doi.org/10.1021/acs.jpca.5b05080.

[43] Limão-Vieira P, Vasekova E, Raja Sekhar BN, Mason NJ, Hoffmann S V. VUV photo-absorption spectroscopy of vinyl chloride studied by high resolution synchrotron

radiation. Chem Phys 2006;330:265–74. https://doi.org/10.1016/j.chemphys.2006.08.021.

[44] Mason NJ, Dawes A, Mukerji R, Drage EA, Vasekova E, Webb SM, et al. Atmospheric chemistry with synchrotron radiation. J Phys B At Mol Opt Phys 2005;38:S893–911. https://doi.org/10.1088/0953-4075/38/9/027.

[45] Marom R, Golan A, Rosenwaks S, Bar I. Photodissociation dynamics of vibrationally excited CH2Cl2 molecules. Chem Phys Lett 2003;378:305–12. https://doi.org/10.1016/j.cplett.2003.07.012.

[46] Werner H-J, Knowles PJ, Knizia G, Manby FR, Schütz M, Celani P, et al. MOLPRO, version 2015.1 2015.

[47] Watts JD, Gauss J, Bartlett RJ. Coupled-cluster methods with noniterative triple excitations for restricted open-shell Hartree-Fock and other general single determinant reference functions. Energies and analytical gradients. J Chem Phys 1993;98:8718–33. https://doi.org/10.1063/1.464480.

[48] Wilson AK, van Mourik T, Dunning Jr. TH. Sextuple zeta correlation consistent basis sets for boron through neon. Comp Theor Chem 1996;388:339–49.

[49] Schaftenaar G, Noordik JH. Molden: A pre- and post-processing program for molecular and electronic structures. J Comput Aid Mol Des 2000;14:123–34. https://doi.org/10.1023/A:1008193805436.

[50] Korona T, Werner HJ. Local treatment of electron excitations in the EOM-CCSD method. J Chem Phys 2003;118:3006–19. https://doi.org/10.1063/1.1537718.

[51] Kaufmann K, Baumeister W, Jungen M. Universal Gaussian basis sets for an optimum representation of Rydberg and continuum wavefunctions. J Phys B At Mol Opt Phys 1989;22:2223–40. https://doi.org/10.1088/0953-4075/22/14/007.

[52] Knowles PJ, Hampel C, Werner HJ. Coupled cluster theory for high spin, open shell reference wave functions. J Chem Phys 1993;99:5219–27. https://doi.org/10.1063/1.465990.

[53] Eden S, Limão-Vieira P, Hoffmann S V., Mason NJ. VUV photoabsorption in CF3X (X = Cl, Br, I) fluoro-alkanes. Chem Phys 2006;323:313–33.

[54] Brownsword RA, Hillenkamp M, Laurent T, Vatsa RK, Volpp HR, Wolfrum J. Dynamics of H atom formation in the photodissociation of chloromethanes at 193.3 nm. J Phys Chem A 1997;101:5222–7. https://doi.org/10.1021/jp963811r.

[55] Werner H-J. Third-order multireference perturbation theory The CASPT3 method. Mol Phys 1996;89:645–61. https://doi.org/10.1080/002689796173967.

[56] Celani P, Werner H-J. Multireference perturbation theory for large restricted and selected active space reference wave functions. J Chem Phys 2000;112:5546–57. https://doi.org/10.1063/1.481132.

[57] Werner H-J, Knowles PJ. A comparison of variational and non-variational internally contracted multiconfiguration-reference configuration interaction calculations. Theor Chim Acta 1990;78:175–87. https://doi.org/10.1007/BF01112867.

[58] Kato H, Masui H, Hoshino M, Cho H, Ingólfsson O, Brunger MJ, et al. A-band methyl halide dissociation via electronic curve crossing as studied by electron energy loss spectroscopy. J Chem Phys 2010;133:054304. https://doi.org/10.1063/1.3464483.

[59] Brunger MJ. Electron scattering and transport in biofuels, biomolecules and biomass fragments. Int Rev Phys Chem 2017;36:333–76. https://doi.org/10.1080/0144235X.2017.1301030.

[60] Koopmans T. Über die Zuordnung von Wellenfunktionen und Eigenwerten zu den Einzelnen Elektronen Eines Atoms. Physica 1934;1:104–13. https://doi.org/10.1016/S0031-8914(34)90011-2.

[61] Robin MB. Higher Excited States of Polyatomic Molecules, Volume I. Academic Press; 1974.

[62] Chemical Kinetics and Photochemical Data for Use in Stratospheric Modelling, Evaluation number 12, NASA, Jet Propulsion Laboratory, JPL, Publication 97-4, January 15. 1997.

[63] Limão-Vieira P, Eden S, Kendall PA, Mason NJ, Hoffmann S V. VUV photo-absorption cross-section for CCl2F2. Chem Phys Lett 2002;364:535–41. https://doi.org/10.1016/S0009-2614(02)01304-0.

Figure captions

Fig. 1. Ground state geometry at the CCSD(T)level with the aug-cc-pV5Z basis set for dichloromethane. Bond lengths are in Å and angles in (°).

Fig. 2. High-resolution VUV photoabsorption spectrum of dichloromethane in the 5.8–10.8 eV photon energy range. See text for details.

Fig. 3. VUV photoabsorption spectrum of dichloromethane in the 7.4–8.6 eV photon energy range. See text for details.

Fig. 4. VUV photoabsorption spectrum of dichloromethane in the 8.5–9.7 eV photon energy range. See text for details.

Fig. 5. VUV photoabsorption spectrum of dichloromethane in the 9.6–10.8 eV photon energy range. See text for details.

Fig. 6. PECs for the ground and low-lying excited singlet states of CH_2Cl_2 plotted as a function of $R_{C\text{–}Cl}$, calculated at the EOM-CCSD/ aug-cc-pV5Z(g)+R level of theory in the C_s symmetry group. Labelling on the right vertical axis relates to the four lowest-lying A′ and A″ states. See text for details.

Table captions

Table 1. Calculated geometry of CH_2Cl_2 compared with previous works. Bond lengths are in Å and angles in (°).

Table 2. Calculated vertical excitation energies (EOM-CCSD/aug-cc-pV5Z(g)+R) and oscillator strengths (singlet and triplet states) of CH_2Cl_2 compared with experimental data (energies in eV). See text for details.

Table 3. Calculated vertical excitation energies using multiconfigurational methods (CASPT2 and MRCI) on the lowest lying singlet and triplet valence states of CH_2Cl_2 (energies in eV). See text for details.

Table 4. Calculated vertical ionisation energies (CCSD(T) geometry with aug-cc-pV5Z basis set) and intensities (pole strengths, PS) compared with experimental values for CH_2Cl_2 (in eV).

Table 5. Proposed vibrational assignments of the CH_2Cl_2 absorption bands in the photon energy range 7.4–8.6 eV[a]. Energies in eV.

Table 6. Proposed vibrational assignments of the CH_2Cl_2 absorption bands in the photon energy range 8.5–9.7 eV[a]. Energies in eV.

Table 7. Proposed vibrational assignments of the CH_2Cl_2 absorption bands in the photon energy range 9.6–10.8 eV[a]. Energies in eV.

Table 8. Energy value (eV), quantum defect (δ) and assignment of the Rydberg series converging to the ionic electronic ground ($3b_1^{-1}$), first ($7b_2^{-1}$), second ($2a_2^{-1}$) and third ($9a_1^{-1}$) excited states of dichloromethane, CH_2Cl_2[a].

Table 9. Calculations of the potential energy curves, along one of the C–Cl bonds, of the four lowest-lying A′ and A″ states performed with MOLPRO at the EOM-CCSD/aug-cc-pV5Z(g)+R level of theory in the C_s symmetry group. The other geometry parameters were kept fixed at their values obtained at the CCSD(T)/aug-cc-pV5Z level.

Fig. 1. Ground state geometry at the CCSD(T) level with the aug-cc-pV5Z basis set for dichloromethane. Bond lengths are in Å and angles in (°).

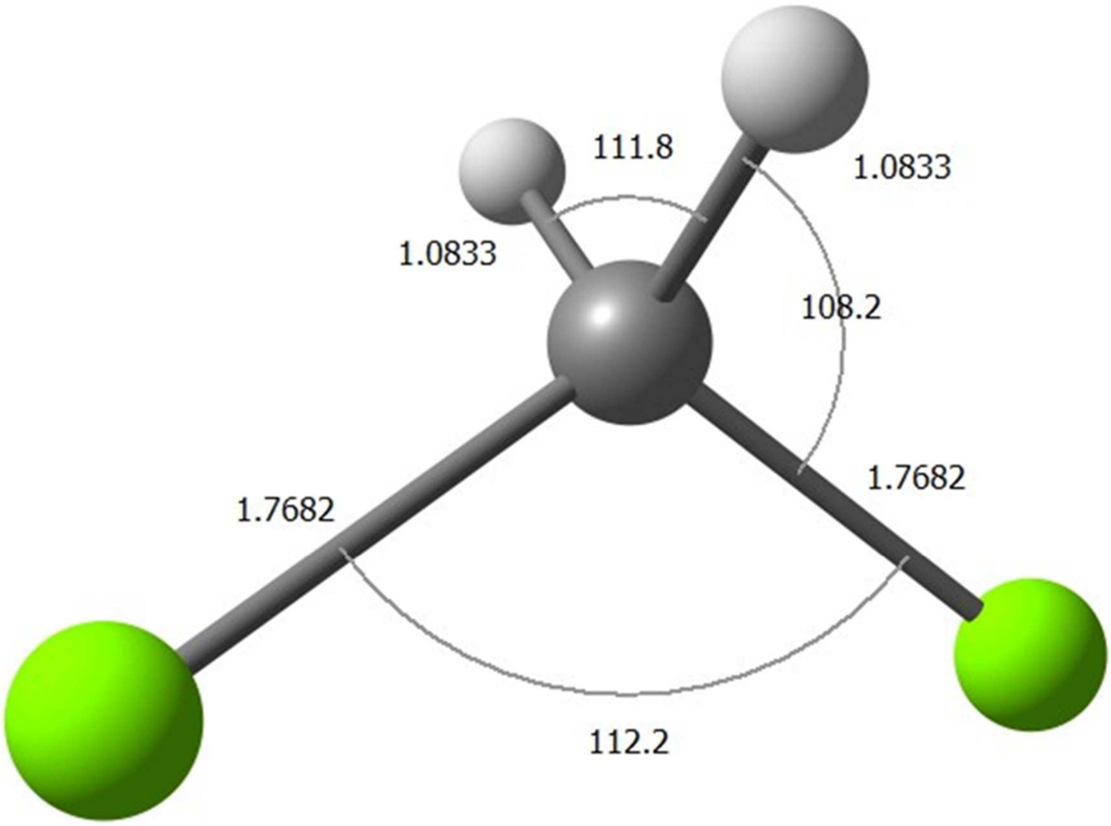

Fig. 2. High-resolution VUV photoabsorption spectrum of CH_2Cl_2 in the 5.8–10.8 eV photon energy range. See text for details.

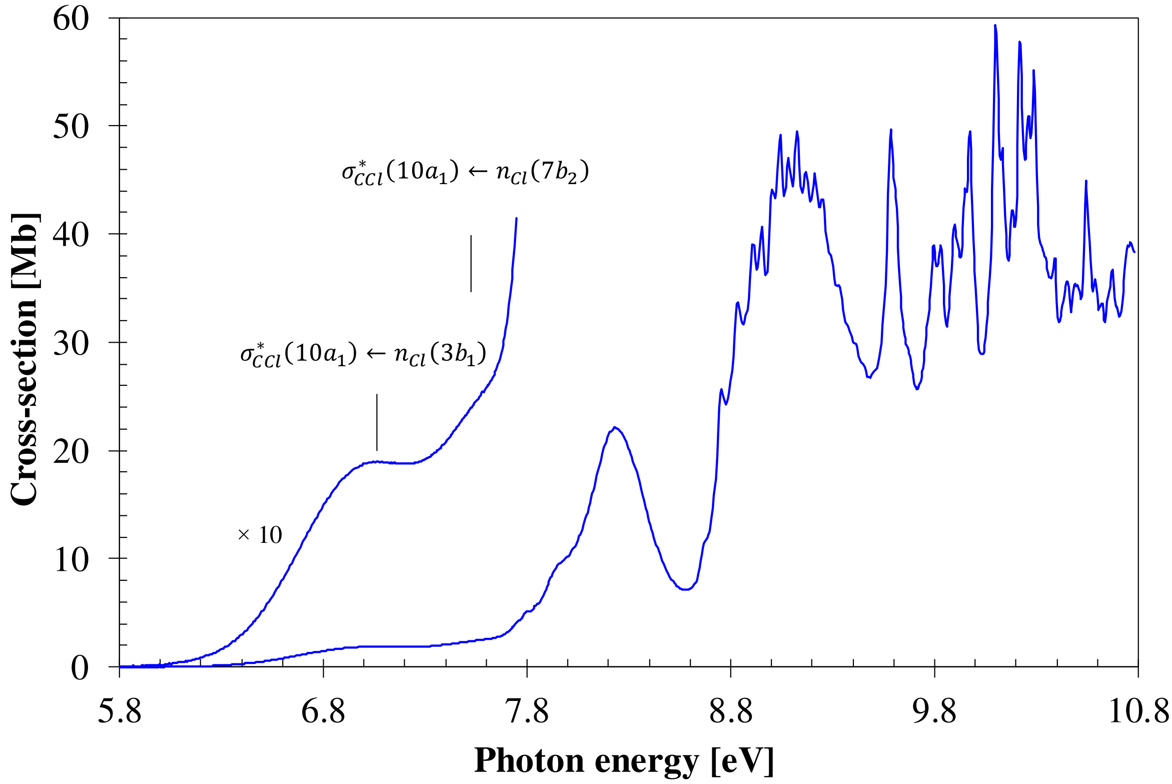

Fig. 3. VUV photoabsorption spectrum of CH_2Cl_2 in the 7.4–8.6 eV photon energy range. See text for details.

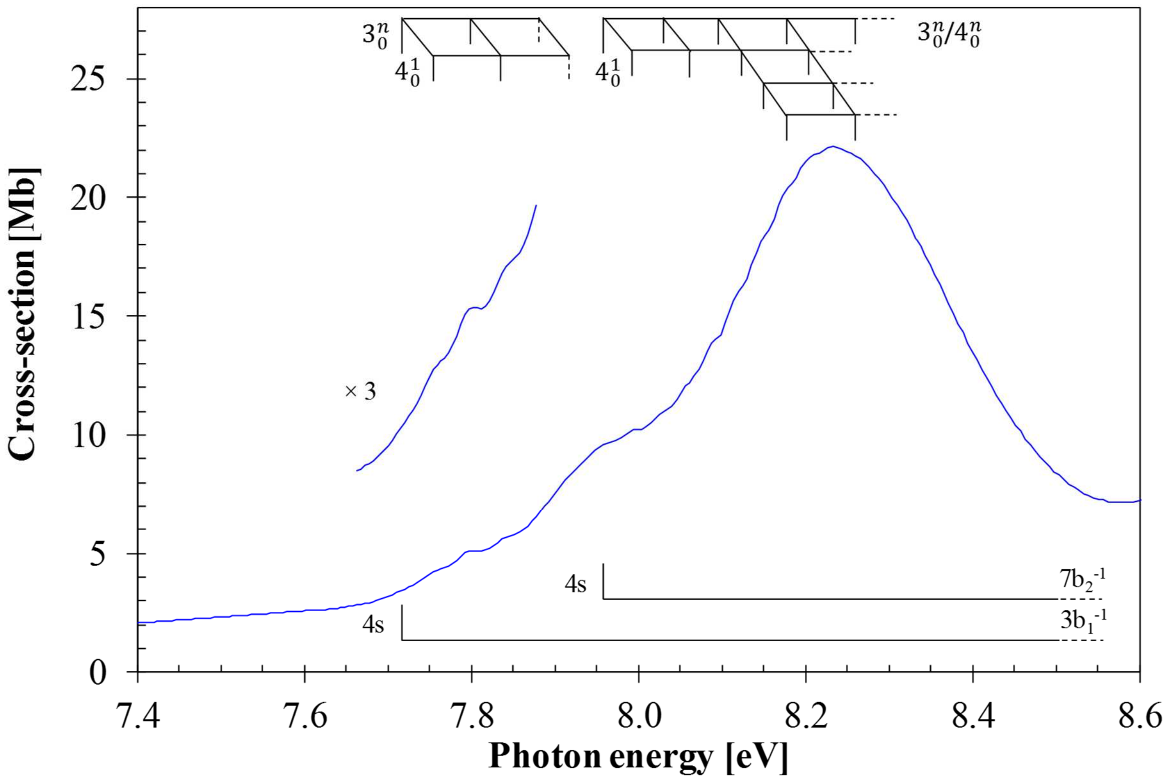

Fig. 4. VUV photoabsorption spectrum of CH_2Cl_2 in the 8.5–9.7 eV photon energy range. See text for details.

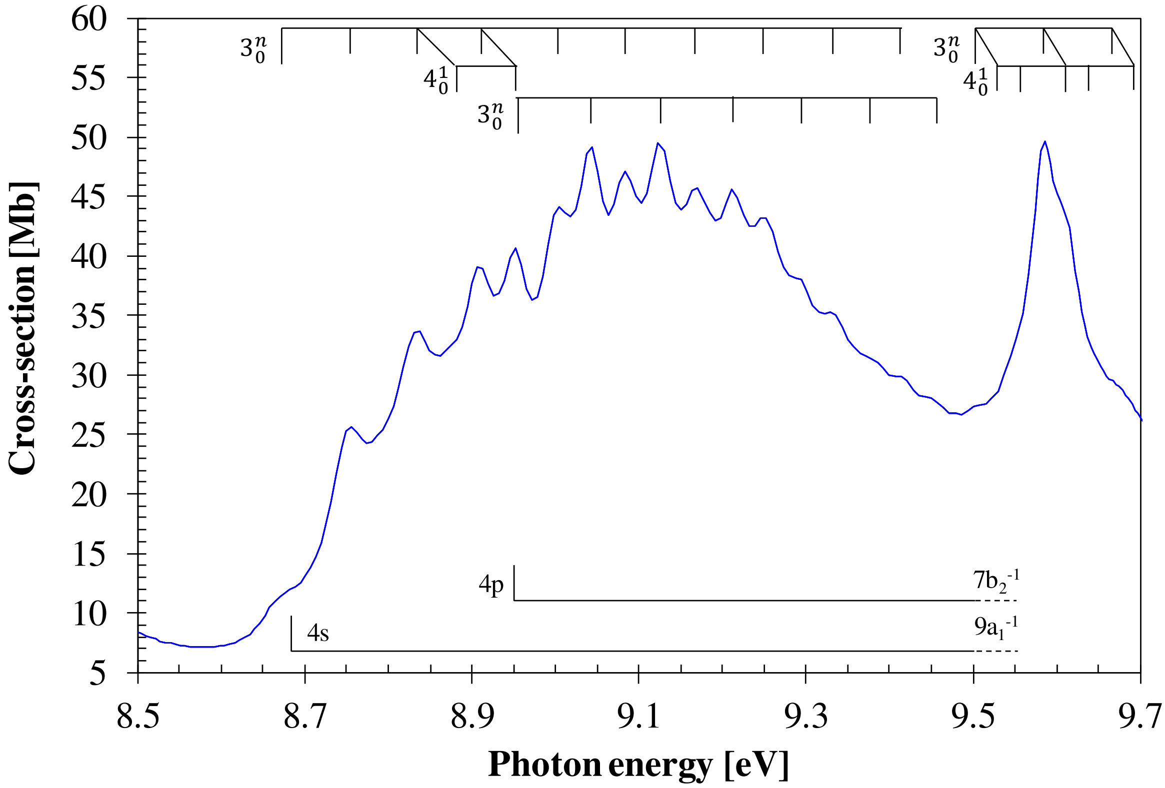

Fig. 5. VUV photoabsorption spectrum of CH_2Cl_2 in the 9.6–10.8 eV photon energy range. See text for details.

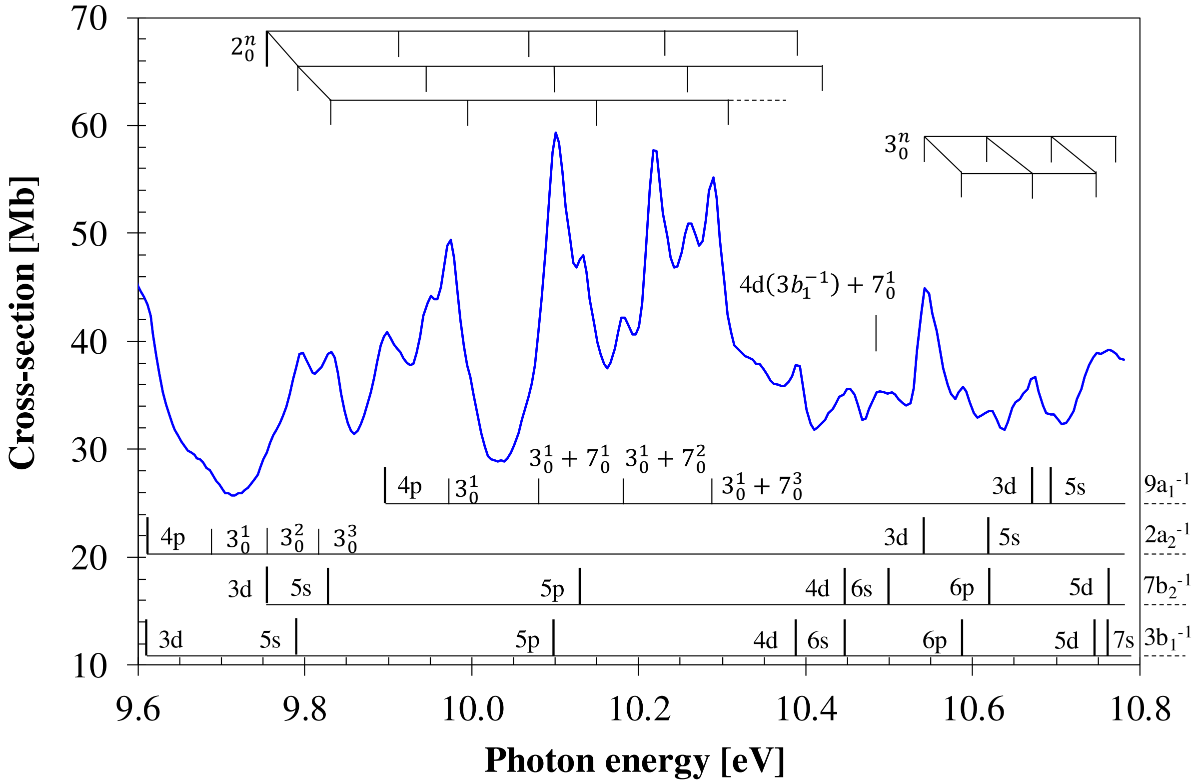

Fig. 6. PECs for the ground and low-lying excited singlet states of CH_2Cl_2 plotted as a function of $R_{C–Cl}$, calculated at the EOM-CCSD/ aug-cc-pV5Z(g)+R level of theory in the C_s symmetry group. Labelling on the right vertical axis related to the four lowest-lying A′ and A″ states. See text for details.

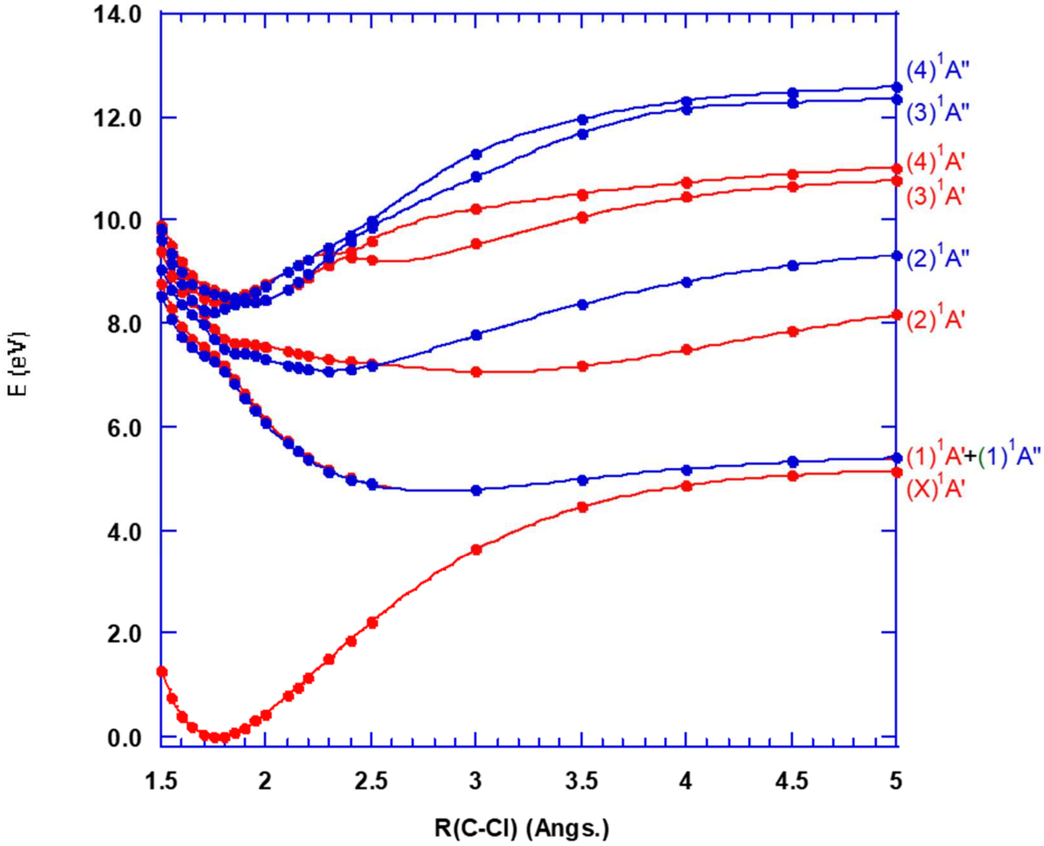

Table 1. Calculated geometry of CH_2Cl_2 compared with previous works. Bond lengths are in Å and angles in (°).

	This work	[10]	[38]	Exp. [7]
	CCSD(T) aug-cc-pV5Z	PBE0 aug-cc-pV5Z	CASPT2 ANO-L	
R(CH)	1.0721	1.084	1.080	1.0874
R(CCl)	1.7686	1.761	1.7631	1.7648
∡ HCH	111.7	111.4	111.1	111.51
∡ ClCCl	112.5	112.9	112.8	112.03
∡ HCCl	108.2	108.1	–	–

Table 2. Calculated vertical excitation energies (EOM-CCSD/aug-cc-pV5Z(g)+R) and oscillator strengths (singlet and triplet states) of CH_2Cl_2 compared with experimental data (energies in eV). See text for details.

State	E (eV)	f_L	$\langle r^2 \rangle^a$	HOMO (3b$_1$), n_{Cl}	HOMO-1 (7b$_2$), n_{Cl}	HOMO-2 (9a$_1$), n_{Cl}	HOMO-3 (2a$_2$), n_{Cl}	Mixed character	E (eV) expt.	Cross section (Mb)
$\tilde{X}\ ^1A_1$										
	7.188	0.00024	77	σ_{CCl}*(10a$_1$)					7.069	1.9
	7.316	0.01178	76		σ_{CCl}*(10a$_1$)				7.519	2.4
	7.607		76					(3b$_1$) → σ_{CCl}*(8b$_2$) + (2a$_2$)→ σ_{CCl}*(10a$_1$)		
	7.815	0.00467	77					(9a$_1$) → σ_{CCl}*(10a$_1$) + (7b$_2$) → σ_{CH}*(11a$_1$)	7.793	5.0
	8.232	0.04125	102	4s(a$_1$)					7.72(0)	3.5
	8.389	0.04708	103		4s(a$_1$)				7.96(3) / 8.233	9.6 / 22.2
	8.535		96					(3b$_1$) → σ_{CCl}*(8b$_2$) + (2a$_2$) → 4s(a$_1$)		
	8.592	0.01394	95			4p(a$_1$)			9.899	40.8
	9.112	0.03443	120	4p(b$_1$)					8.837	33.6
	9.141		92					(2a$_2$) → 4s(a$_1$) + (3b$_1$) → σ_{CCl}*(8b$_2$)		
	9.203	0.00701	96			4s(a$_1$)			8.67(6) / 8.756	11.6 / 25.7
	9.254		123		4p(b$_1$)					
	9.299	0.02407	118	4p(a$_1$)					9.294	37.9
	9.342	0.03129	99					(3b$_1$) → σ_{CH}*(11a$_1$) + (2a$_2$) → σ_{CCl}*(10a$_1$)	9.123	49.5
	9.384	0.00805	130		4p(a$_1$)				8.952	40.6
	9.524	0.21028	96			σ_{CCl}*(8b$_2$)			9.585	49.7
	9.682		145	4p(b$_2$)						
	9.749	0.00503	127					(2a$_2$) → 4p(b$_1$) + (3b$_1$) → 3d(a$_2$)		
	9.756	0.01438	149		4p(b$_2$)				9.75(9)	30.6

9.762	0.00011	136					$(9a_1) \rightarrow 4p(b_1) + (3b_1) \rightarrow 5s(a_1)$		
9.776	0.00158	142					$(3b_1) \rightarrow 5s(a_1) + (9a_1) \rightarrow 4p(b_1)$	9.793	38.8
9.851		143					$(2a_2) \rightarrow 4p(a_1) + (3b_1) \rightarrow 3d(b_2)$		
9.884	0.04741	154		$3d(a_1)$				9.75(9)	30.6
9.914	0.01322	142					$(9a_1) \rightarrow 3d(a_1) + (7b_2) \rightarrow 3d(b_2)$		
10.024	0.02223	169					$(3b_1) \rightarrow 3d(a_1) + (2a_2) \rightarrow 4p(b_2)$		
10.059	0.00242	172	$3d(b_1)$					9.61(1)	43.4
10.087	0.05586	167					$(7b_2) \rightarrow 3d(a_1) + (9a_1) \rightarrow 4p(b_2)$		
10.108		163		$3d(b_1)$					
10.210		178					$(3b_1) \rightarrow 3d(b_2) + (2a_2) \rightarrow 4p(a_1)$		
10.220	0.00008	269	$3d(a_1)$						
10.254	0.04096	182					$(7b_2) \rightarrow 3d(b_2) + (9a_1) \rightarrow 3d(a_1)$		
10.259	0.00077	203					$(3b_1) \rightarrow 3d(a_2) + (2a_2) \rightarrow 4p(b_1)$		
10.285	0.00983	198		$3d(a_2)$					
10.322	0.03844	276		$5s(a_1)$				9.828	38.8
10.433	0.00993	356	$5p(b_1)$					10.101	59.3
10.462	0.02305	345	$5p(a_1)$					10.264	50.8
10.492		174				$3d(a_1)$			
10.495	0.02537	211					$(9a_1) \rightarrow 4p(b_2) + (7b_2) \rightarrow 3d(a_2)$		
10.500	0.01345	163			$3d(a_1)$			10.670	36.5
10.506	0.00137	261					$(2a_2) \rightarrow 4p(b_2) + (3b_1) \rightarrow 3d(a_1)$		
10.513		358		$5p(b_1)$					
10.536		393	$5p(b_2)$						
10.542	0.00020	377		$5p(a_1)$				10.134	47.9
10.613	0.00704	396		$5p(b_2)$				10.454	35.6

10.629	0.00006	440	4d(a_1)						
10.684	0.00014	234					($2a_2$) → 3d(b_1) + ($7b_2$) → 6s(a_1)		
10.706	0.01066	184			3d(b_1)				
10.716	0.00658	380					($7b_2$) → 6s(a_1) + ($2a_2$) → 3d(b_1)		
10.730	0.00048	491	4d(b_1)					10.388	37.8
10.759	0.00003	218				3d(b_2)			
10.762		519	4d(b_2)						
10.768	0.00993	227			3d(b_2)				
10.785		478		4d(b_1)					
10.801	0.00722	574				3d(b_1)			
10.825	0.00002	714	6s(a_1)						
10.826	0.00185	438		4d(b_2)					
10.832	0.00385	296				3d(a_2)			
10.839	0.00061	594	5d(a_1)						
10.845		203			3d(a_2)				
10.860	0.00329	570		4d(a_2)					
10.890	0.01102	667		4d(a_1)				10.450	35.6
10.891		497					($2a_2$) → 5s(a_1) + ($3b_1$) → 6p(b_2)		
10.911		256				3d(a_1)			
10.912	0.00000	666		4d(a_1)					
10.917	0.00273	924	6p(b_1)					10.588	35.8
10.929	0.00058	256			5s(a_1)			10.693	33.2
10.932	0.00778	968	6p(a_1)					10.670	36.5
10.937	0.00655	401			6s(a_1)				
10.989		939		6p(b_1)					
10.993		845					($3b_1$) → 6p(b_2) + ($2a_2$) → 5s(a_1)		

10.997	0.00117	967		$6p(a_1)$			10.620	33.5
11.020	0.00003	1072	$5d(a_1)$					
11.042	0.00227	928		$6p(b_2)$			10.767	39.1
11.075	0.00079	960	$5d(b_1)$				10.744	35.5
11.089	0.01391	654				$(2a_2) \rightarrow 5p(b_1) + (3b_1) \rightarrow 4d(a_2)$		
11.092	0.01574	956		$6s(a_1)$			10.503	35.3
11.099		866				$(3b_1) \rightarrow 5d(b_2) + (2a_2) \rightarrow 5p(a_1)$		
11.119	0.00007	717			$5p(b_1)$			
11.124	0.00161	1324	$6s(a_1)$				10.454	35.6
11.127		887		$5d(b_1)$				
11.150	0.00486	689				$(9a_1) \rightarrow 5p(a_1) + (7b_2) \rightarrow 5d(b_2)$		
11.152	0.01140	912	$5d(a_1)$					
11.157		925				$(2a2) \rightarrow 5p(a_1) + (3b_1) \rightarrow 5d(b_2)$		
11.173	0.00098	1653	$7p(a_1)$					
11.175	0.04823	440				$(9a_1) \rightarrow 5p(b_2) + (7b_2) \rightarrow 7s(a_1)$		
11.179	0.00203	1574	$7p(b_1)$					
11.190	0.00473	1505		$5d(a_1)$			10.767	39.1
11.201	0.02308	1043				$(7b_2) \rightarrow 5d(b_2) + (9a_1) \rightarrow 5p(a_1)$		
11.216	0.00006	695				$(3b_1) \rightarrow 4d(a_2) + (2a_2) \rightarrow 5p(b_1)$		
11.225	0.00169	1510		$5d(a_1)$				
11.237		1316	$7p(b_2)$					
11.243		1642		$7p(b_1)$				
11.256	0.00005	2440	$7s(a_1)$				10.767	39.1
11.260	0.00488	866		$5d(a_2)$				
11.268	0.00928	1070		$7p(a_1)$				

11.291	0.00148	1387		$7p(b_2)$			
11.301	0.00828	551					$(2a_2) \rightarrow 5p(b_2) + (3b_1) \rightarrow 6d(a_1)$
11.322		487				$6s(a_1)$	
11.325	0.00150	1889				$6p(b_1)$	
11.331	0.00415	492			$4d(a_1)$		
11.335	0.02658	1030					$(2a_2) \rightarrow 4d(b_1) + (9a_1) \rightarrow 4d(b_2)$
11.372	0.00014	796	$6d(b_1)$				
11.389	0.00619	590					$(2a_2) \rightarrow 4d(b_2) + (3b_1) \rightarrow 6d(a_1) + (9a1) \rightarrow 4d(b_1)$
11.397	0.00048	643					$(9a_1) \rightarrow 5d(b_1) + (3b_1) \rightarrow 6d(a_1)$
11.412		689		$6d(b_1)$			
11.420	0.00001	1580	$8s(a_1)$				
11.422	0.03931	498					$(2a_2) \rightarrow 5d(b_1) + (9a_1) \rightarrow 4d(b_2)$
11.431		990	$8p(b_2)$				
11.431	0.00722	657					$(7b_2) \rightarrow 8s(a_1) + (9a_1) \rightarrow 5p(b_2)$
11.437	0.00476	1063	$8p(b_1)$				
11.449	0.00774	1155	$8p(a_1)$				
11.473		691				$4d(a_1)$	
11.479	0.00692	867					$(9a_1) \rightarrow 4d(a_1) + (7b_2) \rightarrow 6d(b_2)$
11.493	0.00036	1531		$6d(a_1)$			
11.499		950					$(2a_2) \rightarrow 4d(a_1) + (9a_1) \rightarrow 4d(a_2)$
11.515	0.00132	755					$(7b_2) \rightarrow 6d(b_2) + (9a_1) \rightarrow 4d(a_1)$
11.519		798				$7s(a_1)$	
11.520	0.00165	1230		$6d(a_1)$			
11.521	0.00087	709			$6p(a_1)$		
11.545		904					$(9a_1) \rightarrow 4d(a_2) + (2a_2) \rightarrow 4d(a_1)$

11.581	0.00142	917	9s(a_1)			
11.595	0.00598	904			7p(b_1)	
11.599		894			7p(a_1)	
11.611	0.00025	905		6p(b_1)		
11.669		770				($2a_2$) → 8s(a_1) + ($3b_1$) → 9p(b_2)

[a] Mean value of r^2 (electronic radial spatial extents)

Table 3. Calculated vertical excitation energies using multiconfigurational methods (CASPT2 and MRCI) on the lowest lying singlet and triplet valence states of CH_2Cl_2 (energies in eV). See text for details.

Lowest lying singlet valence states (values in brackets are calculated oscillator strengths)

Energy (eV)	$^1B_1$	$^1B_2$	$^1A_2$	$^1A_1$
TD-PBE0/aug-cc-pV5Z [10]	6.694 (<0.001)	6.998 (0.014)		7.472 (0.003)
MS-CASPT2(12,10)/ANORCC [39]	6.71 (0.007)	6.80 (0.022)		
SO-MS-CASPT2(12,10)/ANORCC [39]	7.01	7.06		
EOM-CCSD/aug-cc-pV5Z(g)+R [a]	7.188 (0.00024)	7.316 (0.01178)	7.607	7.815 (0.00467)
MS-CAS(20,14)/aug-cc-pV5Z(g) [a]	8.017 (0.014)	8.016 (0.011)	8.337	8.623 (0.006)
MS-CASPT2(20,14)/aug-cc-pV5Z(g) [a]	7.168	7.325	7.656	7.869
MS-CAS(20,14)+icMRCI+Q/aug-cc-pV5Z(g) [a]	7.304	7.421	7.742	7.897
Present experiment	7.069	7.519		7.96(3) / 8.233

Lowest lying triplet valence states

Energy (eV)	$^3B_1$	$^3B_2$	$^3A_2$	$^3A_1$
MS-CASPT2(12,10)/ANORCC [39]	6.180	6.230		6.490
SO-MS-CASPT2(12,10)/ANORCC [39]	6.350	6.540	6.770	
EOM-CCSD/aug-cc-pV5Z(g)+R [b]	6.605	6.614	6.920	7.056
MS-CAS(20,14)/aug-cc-pV5Z(g) [a]	7.201	7.057	7.449	7.555
MS-CASPT2(20,14)/aug-cc-pV5Z(g) [a]	6.644	6.611	6.982	7.114
MS-CAS(20,14)+icMRCI+Q/aug-cc-pV5Z(g) [a]	6.750	6.706	7.066	7.186

[a] This work, Molpro 2015.1; [b] This work, Gaussian 09 Rev. E.01

Table 4. Calculated vertical ionisation energies (CCSD(T) geometry with aug-cc-pV5Z basis set) and intensities (pole strengths, PS) compared with experimental values for CH_2Cl_2 (in eV).

	$^2B_1$ ($3b_1^{-1}$)		$^2B_2$ ($7b_2^{-1}$)		$^2A_2$ ($2a_2^{-1}$)		$^2A_1$ ($9a_1^{-1}$)		$^2B_2$ ($6b_2^{-1}$)		$^2A_1$ ($8a_1^{-1}$)		$^2B_1$ ($2b_1^{-1}$)	
ROHF	11.536		11.323		12.147		12.104		–		–		–	
RMP2	11.515		11.610		12.235		12.233		–		–		–	
RCCSD	11.739		11.740		12.405		12.396		–		–		–	
RCCSD(T)	11.597		11.666		12.269		12.285		–		–		–	
UCCSD	11.724		11.714		12.389		12.372		–		–		–	
UCCSD(T)	11.585		11.650		12.257		12.269		–		–		–	
		PS		PS		PS		PS		PS		PS		PS
Koopmans	12.147		12.181		12.897		12.827		15.942		16.800		18.437	
OVGF	11.628	0.908	11.705	0.904	12.335	0.902	12.312	0.905	15.313	0.899	15.913	0.895	17.077	0.895
P3	11.521	0.904	11.585	0.901	12.174	0.898	12.233	0.902	15.424	0.892	15.994	0.887	17.150	0.887
P3+	11.493	0.904	11.561	0.901	12.204	0.901	12.151	0.898	15.370	0.891	15.933	0.886	17.056	0.884
Exp. [20]	11.560		11.596		12.187		12.271		~15.10		~15.80		~16.75	
	11.320 [a]		11.357 [a]		12.152 [a]		12.271 [a]		14.856 [a]		–		–	
Exp. [21]	11.0($^2B_2$) [a]		11.317($^2B_1$) [a]		12.15($^2A_1$) [a]		12.25($^2A_2$) [a]							

[a] adiabatic value

Table 5. Proposed vibrational assignments of the CH_2Cl_2 absorption bands in the photon energy range 7.4–8.6 eV[a]. Energies in eV.

This work			
assignment	energy	ΔE (υ_3')	ΔE (υ_4')
($4sa_1 \leftarrow 3b_1$)			
0_0^0	7.72(0)(s)	…	…
4_0^1	7.759	…	0.039
3_0^1	7.808	0.088	…
$3_0^1 + 4_0^1$	7.842	…	0.034
3_0^2	7.87(7)(s)	0.069	…
$3_0^2 + 4_0^1$	7.91(7)(s)	…	0.040
($4sa_1 \leftarrow 7b_2$)			
0_0^0	7.96(3)(s)	…	…
4_0^1	7.98(9)(b)	…	0.026
$4_0^2/3_0^1$	8.02(5)(s)	0.062	0.036
4_0^3	8.06(1)(s)	…	0.036
$4_0^4/3_0^2$	8.08(8)(s)	0.063	0.027
4_0^5	8.12(5)(s)	…	0.037
$4_0^6/3_0^3$	8.15(1)(s)	0.063	0.026
4_0^7	8.18(4)(s)	…	0.033
$4_0^8/3_0^4$	8.21(1)(s)	0.060	0.027
4_0^9	8.23(3)(b)	…	0.022
4_0^{10}	8.26(0)(s)	…	0.027

[a] (s) shoulder structure. (b) broad structure (the last decimal of the energy value is given in brackets for these less-resolved features);

Table 6. Proposed vibrational assignments of the CH_2Cl_2 absorption bands in the photon energy range 8.5–9.7 eV[a]. Energies in eV.

This work				Previous work	
assignment	energy	ΔE (υ3′)	ΔE (υ4′)	Ref. [15]	Ref. [10]
$\sigma^*_{CCl}(10a_1) \leftarrow n_{Cl}(2a_2) + \sigma^*_{CH}(11a_1) \leftarrow n_{Cl}(3b_1)$ / (*nsa₁* ← *9a₁*)					
0^0_0	8.67(6)(s)	…	…	8.670	8.670
3^1_0	8.762	0.086	…	8.756	8.759
3^2_0	8.837	0.075	…	8.837	8.836
$3^2_0 + 4^1_0$	8.87(5)(s)	…	0.038	…	…
3^3_0	8.907	0.070	…	8.913	8.911
$3^3_0 + 4^1_0$	8.952	…	0.045	…	…
3^4_0	9.00(4)(b)	0.097	…	9.003	9.005
3^5_0	9.083	0.079	…	9.086	9.084
3^6_0	9.170	0.087	…	9.168	9.168
3^7_0	9.253	0.083	…	9.255	9.247
3^8_0	9.336	0.083	…	9.339	9.327
3^9_0	9.40(7)(s)	0.071	…	9.423	9.416
($npa_1 \leftarrow 7b_2$)					
0^0_0	8.952	…	…	8.957	8.953
3^1_0	9.043	0.091	…	9.044	9.043
3^2_0	9.123	0.080	…	9.129	9.127
3^3_0	9.211	0.088	…	9.216	9.216
3^4_0	9.287	0.076	…	9.302	9.290
3^5_0	9.37(1)(s)	0.084	…	9.386	9.387
3^6_0	9.45(0)(s)	0.079	…	–	–
($8b_2(\sigma_{CCl}^*) \leftarrow 9a_1$)					
0^0_0	9.508	…	…	–	–
4^1_0	9.53(0)(s)	…	0.022	–	–
4^2_0	9.55(2)(s)	…	0.022	–	–
3^1_0	9.585	0.077	…	–	9.592
$3^1_0 + 4^1_0$	9.60(7)(s)	…	0.022	–	–
$3^1_0 + 4^2_0$	9.63(7)(s)	…	0.030	–	–
3^2_0	9.66(0)(s)	0.075	…	–	9.676
$3^2_0 + 4^1_0$	9.69(4)(s)	…	0.034	–	–

[a] (s) shoulder structure. (b) broad structure (the last decimal of the energy value is given in brackets for these less-resolved features);

Table 7. Proposed vibrational assignments of the CH_2Cl_2 absorption bands in the photon energy range 9.6–10.8 eV[a]. Energies in eV.

This work					Previous work	
assignment	energy	ΔE (υ_2')	ΔE (υ_3')	ΔE (υ_7')	Ref. [15]	Ref. [10]
4p $(2a_2)^{-1}$ / 3d $(3b_1)^{-1}$	9.61(1)	…	…	…	…	…
4p + 3_0^1	9.68(6)	…	0.075	…	…	9.676
4p + 3_0^2 / 3d $(7b_2)^{-1}$	9.75(9)(s)	…	0.073	…	…	…
4p + 3_0^3	9.82(4)(s)	…	0.065	…	9.779	9.798
3d $(7b_2)^{-1}$ + 2_0^1	9.91(1)(s)	0.152	…	…	9.911	9.952
3d + 2_0^2	10.07(2)(s)	0.161	…	…	10.020	10.106
3d + 2_0^3	10.23(4)(s)	0.162	…	…	10.151	10.265
3d + 2_0^4 / 4d $(3b_1)^{-1}$	10.388	0.154	…	…	…	…
…	…	…	…	…	9.813	…
5s $(3b_1)^{-1}$ + 2_0^1	9.955	0.162	…	…	9.967	…
5s + 2_0^2	10.101	0.146	…	…	10.081	…
5s + 2_0^3	10.264	0.163	…	…	10.202	…
5s + 2_0^4	10.42(3)(s)	0.159	…	…	10.310	…
5s $(7b_2)^{-1}$	9.828	…	…	…	9.854	…
5s + 2_0^1	9.99(9)(s)	0.171	…	…	9.990	…
5s + 2_0^2	10.15(0)(s,w)	0.151	…	…	10.116	…

5s + 2_0^3	10.30(6)(s,w)	0.156	…	…	10.238	…
4p $(9a_1)^{-1}$ + 3_0^1	9.975	…	0.076	…	…	…
4p + 3_0^1 + 7_0^1	10.08(0)(s,w)	…	…	0.105	…	…
4p + 3_0^1 + 7_0^2	10.184	…	…	0.104	…	…
4p + 3_0^1 + 7_0^3	10.289	…	…	0.105	10.281	…
4d $(3b_1)^{-1}$ + 7_0^1	10.485	…	…	0.097	…	…
3d $(2a_2)^{-1}$ + 3_0^1 / 6p $(7b_2)^{-1}$	10.620	…	0.077	…	10.614	…
3d + 3_0^2 / 6p + 3_0^1 / 5s $(2a_2)^{-1}$ / 5s $(9a_1)^{-1}$	10.693	…	0.073	…	10.699	…
3d + 3_0^3 / 6p + 3_0^2	10.77(7)(s,w)	…	0.084	…	10.788	…
6p $(3b_1)^{-1}$ + 3_0^1	10.670	…	0.082	…	…	…
6p + 3_0^2 / 5d $(3b_1)^{-1}$	10.744	…	0.074	…	…	…

[a] (s) shoulder structure. (b) broad structure. (w) weak feature (the last decimal of the energy value is given in brackets for these less-resolved features);

Table 8. Energy value (eV), quantum defect (δ) and assignment of the Rydberg series converging to the ionic electronic ground ($3b_1^{-1}$), first ($7b_2^{-1}$), second ($2a_2^{-1}$) and third ($9a_1^{-1}$) excited states of dichloromethane, CH_2Cl_2[a].

This work			Ref. [10]
E_n	δ	assignment	
IE$_1$ = 11.320 eV $(3b_1)^{-1}$			
($nsa_1 \leftarrow 3b_1$)			
7.72(0)(s)	2.06	4s(a_1)	7.7
9.793	2.01	5s(a_1)	9.798
10.454	2.04	6s(a_1)	10.457
10.767	2.04	7s(a_1)	10.766
($npb_1 \leftarrow 3b_1$) / ($npa_1 \leftarrow 3b_1$)			
8.837 / 9.294	1.66 / 1.41	4p(b_1) / 4p(a_1)	8.670 / …
10.101 / 10.264	1.66 / 1.41	5p(b_1) / 5p(a_1)	10.106 / …
10.588 / 10.670	1.69 / 1.42	6p(b_1) / 6p(a_1)	10.592 / …
($ndb_1 \leftarrow 3b_1$)			
9.61(1)(s)	0.18	3d(b_1)	9.617
10.388	0.18	4d(b_1)	10.397
10.744	0.14	5d(b_1)	10.742
IE$_2$ = 11.357 eV $(7b_2)^{-1}$			
($nsa_1 \leftarrow 7b_2$)			
7.96(3)(s)	1.99	4s(a_1)	7.985
9.828	2.01	5s(a_1)	9.835
10.503	2.00	6s(a_1)	10.491
($npa_1 \leftarrow 7b_2$) / ($npb_2 \leftarrow 7b_2$)			
8.952 / 9.75(9)(s)	1.62 / 1.08	4p(a_1) / 4p(b_2)	8.953 / …
10.134 / 10.454	1.66 / 1.12	5p(a_1) / 5p(b_2)	10.138 / …
10.620 / 10.767	1.70 / 1.19	6p(a_1) / 6p(b_2)	10.624 / …
($nda_1 \leftarrow 7b_2$)			
9.75(9)(s)	0.08	3d(a_1)	9.765
10.450	0.13	4d(a_1)	10.457
10.767	0.19	5d(a_1)	10.787

IE$_3$ = 12.152 eV $(2a_2)^{-1}$			
($nsa_1 \leftarrow 2a_2$)*			
8.67(6)	2.02	4s(a_1)	8.225
10.620	2.02	5s(a_1)	10.491
($npa_1 \leftarrow 2a_2$)*			
9.61(1)(s)	1.68	4p(a_1)	9.592
($nda_1 \leftarrow 2a_2$)*			
10.543	0.09	3d(a_1)	10.546
IE$_4$ = 12.271 eV $(9a_1)^{-1}$			
($nsa_1 \leftarrow 9a_1$)			
8.67(6) / 8.756	2.05 / 2.03	4s(a_1)	8.225
10.693	2.06	5s(a_1)	10.508
($npa_1 \leftarrow 9a_1$)			
9.899	1.60	4p(a_1)	9.902
($nda_1 \leftarrow 9a_1$)			
10.670	0.08	3d(a_1)	10.677

[a] (s) shoulder structure (the last decimal of the energy value is given in brackets for these less-resolved features); * dipole forbidden transition which is part of the vibronic transitions and/or superposition with other Rydberg series.

Table 9. Calculations of the potential energy curves, along one of the C–Cl bonds of the four lowest-lying A′ and A″ states, as performed with MOLPRO at the EOM-CCSD/aug-cc-pV5Z(g)+R level of theory in the C_s symmetry group. The other geometric parameters were kept fixed at their values obtained from the CCSD(T)/aug-cc-pV5Z level.

State character			Type of transition
E (eV)	C_{2v}	C_s	
	$(\tilde{X})^1A_1$	$(\tilde{X})^1A'$	
7.188	$(1)^1B_1$	$(1)^1A'$	n_{Cl} $(3b_1) \rightarrow \sigma_{CCl}^*$ $(10a_1)$
7.316	$(1)^1B_2$	$(1)^1A''$	n_{Cl} $(7b_2) \rightarrow \sigma_{CCl}^*$ $(10a_1)$
7.607	$(1)^1A_2$	$(2)^1A''$	n_{Cl} $(3b_1) \rightarrow \sigma_{CCl}^*$ $(8b_2)$ + n_{Cl} $(2a_2) \rightarrow \sigma_{CCl}^*$ $(10a_1)$
7.815	$(1)^1A_1$	$(2)^1A'$	n_{Cl} $(9a_1) \rightarrow \sigma_{CCl}^*$ $(10a_1)$ + n_{Cl} $(7b_2) \rightarrow \sigma_{CH}^*$ $(11a_1)$
8.232	$(2)^1B_1$	$(3)^1A'$	n_{Cl} $(3b_1) \rightarrow 4s(a_1)$
8.389	$(2)^1B_2$	$(3)^1A''$	n_{Cl} $(7b_2) \rightarrow 4s(a_1)$
8.535	$(1)^1A_2$	$(4)^1A''$	n_{Cl} $(3b_1) \rightarrow \sigma_{CCl}^*$ $(8b_2)$ + n_{Cl} $(2a_2) \rightarrow 4s(a_1)$
8.592	$(2)^1A_1$	$(4)^1A'$	n_{Cl} $(9a_1) \rightarrow 4p(a_1)$[#]

[#] such assignment is only valid for vertical transitions, whereas when the bond is cleavage, the Rydberg character vanishes and all states become valence antibonding.